Functional Materials Letters
Vol. 14, No. 6 (2021) 2150024 (5 pages)
© World Scientific Publishing Company
DOI: 10.1142/S1793604721500247

World Scientific
www.worldscientific.com

Funct. Mater. Lett. 2021.14. Downloaded from www.worldscientific.com
by ZHEJIANG UNIVERSITY OF TECHNOLOGY on 11/22/21. Re-use and distribution is strictly not permitted, except for Open Access articles.

Three-dimensional chitosan/graphene aerogel with vertical alignment for high-performance all-solid-state supercapacitors

Xing Wang,* Yanyu Zhang,* Jing Jin,† Huaping Wu†
and Aiping Liu*,‡

*Key Laboratory of Optical Field Manipulation of Zhejiang Province
Zhejiang Sci-Tech University, Hangzhou 310018, P. R. China
†Key Laboratory of Special Purpose Equipment and Advanced Processing Technology
Ministry of Education and Zhejiang Province
College of Mechanical Engineering, Zhejiang University of Technology
Hangzhou 310023, P. R. China
‡liuaiping1979@gmail.com

Received 1 April 2021; Accepted 30 May 2021 Published 23 June 2021

With the continuous depletion of fossil energy, emerging energy storage equipment based on supercapacitors has been developed rapidly due to their high energy/power density, low cost, long cycle lives and environmental friendliness. The electrode materials of supercapacitors with high specific surface area, porous structure and excellent electrochemical activity are first important and need to be carefully designed. Here, we propose a three-dimensional chitosan/graphene (CS-rGO) aerogel with vertical alignment as the electrodes for the construction of a symmetrical all-solid-state supercapacitor. The unique structures of the aerogel with low density and light mass, direct channel with low tortuosity, high electronic conductivity favor its high volume capacitance of 184.6 mF cm^{-3} at a current density of 2 mA cm^{-3}, high energy density of 32 W h kg^{-1} at power density of 1000 W kg^{-1} and 89.8% retention rate of the volume capacitance after 5000 cycles at 10 mA cm^{-3}. This demonstrates the potential application of CS-rGO aerogel in symmetric supercapacitors (SSCs) for energy storage and conversion.

Keywords: Carbon-based aerogel; all-solid-state supercapacitor; direct channel; porous structure.

The environmental pollution caused by the rapid consumption of fossil fuels conducts people to carry out necessary research on new energy sources including wind energy, hydroelectric power, solar energy, bioenergy and electrochemical energy.[1–3] As one of the new energy storage devices, supercapacitors present a great advantage for use in portable equipment, electric vehicles and stationary energy storage.[4] Carbon-based materials are considered to be the main electrode materials for supercapacitors when considering their high electronic conductivity, good chemical stability, low cost and easy availability.[5–7] Lots of studies have been reported on carbon-based materials with 0D, 1D, 2D and 3D nanostructures. In contrast to 1D and 2D materials, the 3D aerogel network is quite attractive when considering interconnected micro/nanosheets and hierarchical pores with micro, meso and macroscales. Moreover, the ultralow density and flexibility of 3D aerogels are beneficial for portable electronics to afford excellent mechanical stability and high flexural strength.[8–10] For example, Shi *et al*.[11] successfully fabricated mechanically strong, electrically conductive and thermally stable graphene aerogels by a hydrothermal process. Erdem *et al*.[12,13] obtained high-quality 3D graphene networks using Ni foam templates via the ethanol-CVD method. However, the ions and electrons transmission are relatively difficult through the thickness direction in the 3D network with random porous structure.[14] Therefore, an elaborate design for the aerogel materials with directional channels is of critical importance for the performance improvement of supercapacitors.

In this paper, we proposed a lightweight monolithic chitosan/graphene (CS-rGO) aerogel material with vertically arranged network structure, which was further used as electrodes for the construction of a symmetric supercapacitor (SSC). A two-step method of ice template and freeze-drying was introduced to construct the open channels along the growth direction of ice crystals in CS-rGO aerogel. The CS-rGO aerogel had thin thickness, high specific surface area,

‡Corresponding author.

Funct. Mater. Lett. 2021.14. Downloaded from www.worldscientific.com
by ZHEJIANG UNIVERSITY OF TECHNOLOGY on 11/22/21. Re-use and distribution is strictly not permitted, except for Open Access articles.

high electrical conductivity and layered structure, showing high volume capacitance and excellent rate performance. The all-solid-state SSC device based on the CS-rGO aerogel presented high energy/power density and demonstrated great prospects in storage of green and renewable energy.

The synthesis process of all-solid-state SSC with CS-rGO hydrogel as electrodes is shown in Fig. 1(a). The graphene oxide (GO) was first synthesized based on a modified Hummer method.[15] Then a mixed CS (4 g) and GO (1 g) precursor solution was injected into a mold on a copper plate, frozen for 5 min and freeze-dried in an atmosphere of −90 °C to obtain the porous structure with a vertical orientation (ice template method[16,17]). The lyophilized 3D CS-GO scaffolds were annealing treated and carbonized in a furnace with nitrogen atmosphere at 800 °C for 2 h at a heating rate of 5 °C min^{-1}. The ordered CS aerogel was further prepared without the addition of GO in the precursor solution. The disordered CS-rGO (D-CS-rGO) aerogel was also obtained with a similar method when the precursor solution was randomly frozen at −90 °C in a mold without copper plate. In order to assemble the all-solid-state SSC, two CS-rGO electrodes were used as the positive/negative electrodes with the cellulose membrane as the separator, the carbon cloth as the current collector and the PVA/KOH (PVA, polyvinyl alcohol) as the gel electrolyte. The assembled SSC with ultralight quality and small size ($1 \times 1 \times 0.2$ cm^3, Fig. 1(b)) was subsequently maintained at 80 °C overnight to evaporate the excess water in the electrolyte.

The morphology and structure of the products were characterized via field emission scanning electron microscope (FE-SEM, Hitachi S-4800 Japan), X-ray diffractometer (Bruker, D8 Discover), thermogravimetric analyzer (TGA-601, China), Raman spectroscopy (Raman, GS1000 India) and Fourier transformation infrared spectrometer (FTIR, Thermo Scientific iS50, America). The electrochemical performance of a single electrode was studied through a three-electrode setting with the Pt wire as the counter electrode and a saturated calomel electrode (SCE) as the

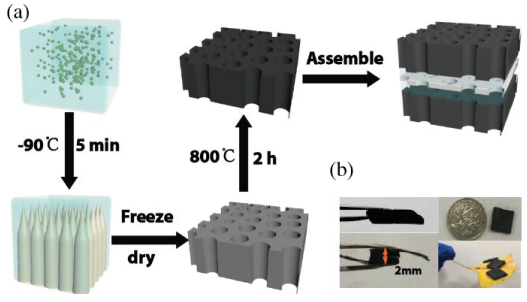

Fig. 1. (a) Schematic illustration of the fabrication of all-solid-state supercapacitors with CS-rGO aerogels as electrode materials. (b) Optical photograph of CS-rGO aerogel and all-solid-state supercapacitors, showing the small size and light mass.

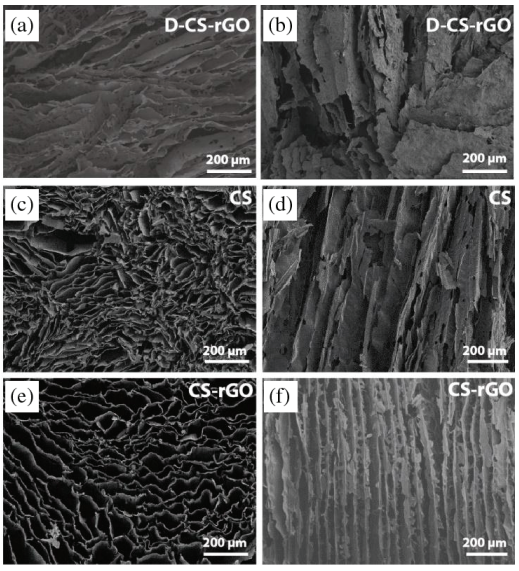

Fig. 2. SEM images of (a), (b) D-CS-rGO aerogel, (c), (d) CS aerogel and (e), (f) CS-rGO aerogel. (a), (c), (e) and (b), (d), (f) are top-view and side-view of samples, respectively.

reference electrode in a 1 M Na_2SO_4 aqueous solution. All electrochemical tests were carried out on the electrochemical workstation (CHI 660E, China), and the cyclic voltammetry (CV) and galvanostatic charge/discharge (GCD) curves were swept from 0 V to 1 V. For electrochemical impedance spectroscopy (EIS) measurement, the amplitude was set to be 5 mV and the frequency was swept from 0.1 Hz to 100 kHz. The volume capacitance C was calculated according to the equation $C = I\Delta t/(S\Delta V)$, where I was the discharge current, Δt was the discharge time, S was the material volume and ΔV was the discharge voltage. The energy density E and powder density P were estimated by using the formula $E = C(\Delta V)^2/2$ and $P = Q\Delta V/2t = E/\Delta t$.

Figure 2 shows the SEM images of D-CS-rGO, CS and CS-rGO aerogels. The D-CS-rGO aerogel presents a disordered structure due to the disordered growth of ice crystals caused by non-directional freezing (Figs. 2(a) and 2(b)). For the ordered CS aerogel prepared by the ice template method, we can see the direct channels from the transverse and longitudinal sections of SEM images (Figs. 2(c) and 2(d)). However, the network structure of CS is friable and collapsed. When the GO is introduced in the CS aerogel, the CS-rGO aerogel remains the directional porous structure unchanged (Fig. 2(f)). The size of the aperture shown in the transverse section is about 10–20 μm (Fig. 2(e)).

Figure 3(a) displays the thermogravimetric analysis of CS and CS-GO aerogels. During the heat treatment, the first reduction of weight in the temperature below 100 °C is related to the water loss, and the fast component loss in the range from 100 °C to 400 °C is the rupture of chemical bond in CS and the loss of carbon oxides. When the temperature

Funct. Mater. Lett. 2021.14. Downloaded from www.worldscientific.com
by ZHEJIANG UNIVERSITY OF TECHNOLOGY on 11/22/21. Re-use and distribution is strictly not permitted, except for Open Access articles.

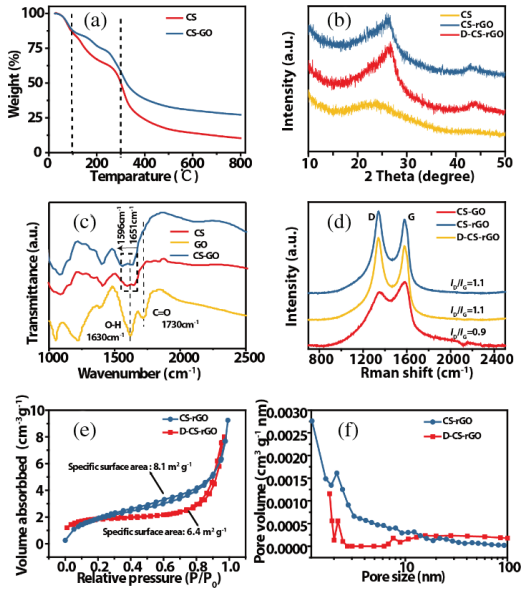

Fig. 3. Structure characterizations of the monolithic aerogels: (a) Thermogravimetric curves of CS and CS-GO aerogels, (b) XRD patterns of CS, D-CS-rGO and CS-rGO aerogels, (c) FTIR spectra of CS, GO and CS-GO aerogels, (d) Raman spectra of D-CS-rGO, CS-rGO and CS-GO aerogels, (e) nitrogen adsorption/desorption isotherm, (f) Pore volume of CS-rGO and D-CS-rGO aerogels.

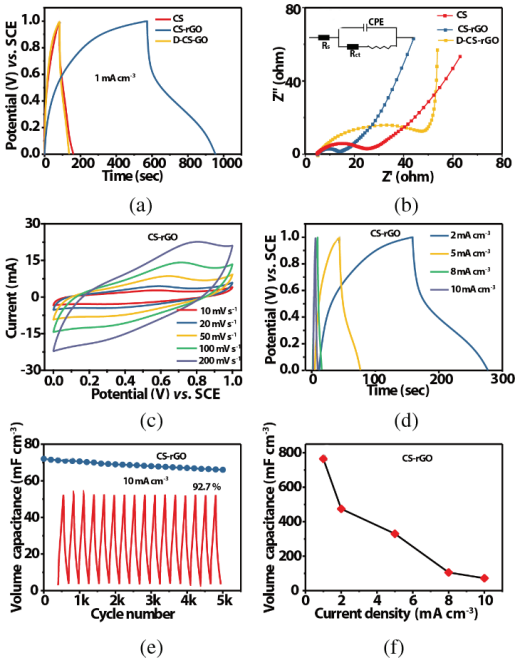

Fig. 4. Electrochemical performance of different electrode: (a) Charge–discharge profiles of D-CS-rGO, CS and CS-rGO aerogels at a constant current density of 1 mA cm^{-3}, (b) EIS spectra of D-CS-rGO, CS and CS-rGO aerogels, (c) CV curves of rGO aerogel at different scanning rates, (d) Charge–discharge profiles of CS-rGO aerogel at different current densities, (e) cycling performance of CS-rGO at 10 $mAcm^{-3}$, (f) Volume capacitance at different current densities for CS- rGO aerogel.

is higher than 400 °C, the quality gradually tends to be stable near 800 °C. This stable temperature is chosen as the annealing temperature of CS-GO aerogel. The XRD results in Fig. 3(b) indicate that after annealing, the CS is transformed into amorphous carbon, giving a broad diffraction peak at about $2\theta = 25°$. The rGO is mainly exfoliated into cumulated flakes in the carbonated CS matrix. [18] In the FTIR spectrum (Fig. 3(c)), the peak at 1730 cm^{-1} and 1630 cm^{-1} for GO is the characteristic of C=O extension and O–H deformation on the carboxyl group. In the CS spectrum, the two characteristic absorption bands at 1651 cm^{-1} and 1596 cm^{-1} are C=O stretching vibration of –NHCO– and –NH– bending vibration of $–NH_2$, respectively. In the CS-GO spectrum, the carboxyl group at 1730 cm^{-1} disappears, and the C=O stretching vibration peak of –NHCO– and the –NH– bending peak of $–NH_2$ move to a lower wave number. The results show that there is an interaction between GO and CS.[19] This means that CS and GO perfectly merge to form a monolithic composite material. The Raman spectrum of CS-rGO in Fig. 3(d) shows two characteristic peaks at 1327 cm^{-1} and 1597 cm^{-1}, corresponding to the D and G bands. In addition, the relative intensity ratio of the D band to the G band (I_D/I_G) for the CS-rGO (D-CS-rGO) aerogel is 1.1, which is greater than that of the CS-GO (I_D/I_G = 0.9), indicating that GO is reduced to rGO under annealing.[20] The BET curve of CS-rGO aerogel presents a typical II isothermal adsorption graph with the measured specific surface area about 8.1 $m^2\ g^{-1}$ (Fig. 3(e)), which is higher than D-CS-rGO (about 6.4 $m^2\ g^{-1}$). The pore diameters of two samples are mainly distributed in 2–10 nm (Fig. 3(f)), indicating that the materials are mainly mesoporous structure.

We also investigated the electrochemical performance of different samples. Figure 4(a) shows the GCD curves of D-CS-rGO, CS and CS-rGO aerogels. According to calculation, the volume capacitance of CS-rGO obtained at a constant current density of 1 mA cm^{-3} is 764.6 mF cm^{-3}, which is about 4 times as much as those of CS and D-CS-rGO aerogels. Figure 4(b) shows the EIS results of three aerogels. The intersection of the semicircular arc and the *x*-axis defined as the equivalent series resistance (R_s) includes the resistances of electrolyte and electrode material itself, and the contact resistance between them. The radius of the semicircular arc represents the transfer resistance (R_{ct}) of the charge during charging–discharging process.[8] By comparison, we can see that the CS-rGO aerogel with well-vertical alignment has the smallest transfer resistance of the charge, indicating its fastest electron transfer during charging-discharging process. The CV curves in Fig. 4(c) show a roughly symmetrical rectangle, which verifies the fast and effective charge transfer of CS-rGO aerogel.[21] It is worth noting that the CS-rGO electrode has a volume capacitance of 764.6, 474.4, 330.0, 105.6 and 72.0 mF cm^{-3} at 1, 2, 5, 8 and 10 mA cm^{-3} (Figs. 4(d) and 4(f)), which is comparable with the recently reported 3D materials (Table 1).[22–26] The volume capacitance obtained

Funct. Mater. Lett. 2021.14. Downloaded from www.worldscientific.com by ZHEJIANG UNIVERSITY OF TECHNOLOGY on 11/22/21. Re-use and distribution is strictly not permitted, except for Open Access articles.

Table 1. Electrochemical performance comparison of recently reported 3D materials.

Electrode material	Electrolyte	Volumn capacitance (mF cm^{-3})	Ref.
B-3D-PCP	1 M Na_2SO_4	715.0	[22]
3DG/CNTCs	1 MH_2SO_4	216.0	[23]
WO_{3-x}/MoO_{3-x}/PANI/carbon	0.1 MNa_2SO_4	216.0	[24]
3D graphene	/	828.1	[25]
Porous carbon	/	20.1	[26]
CS-rGO	1 MNa_2SO_4	764.6	This work

at high current density of 10 mA cm^{-3} retains 92.7% of the initial value after 5000 cycles (Fig. 4(e)), indicating the excellent stability of CS-rGO aerogel.

Considering the superior electrochemical performance, the CS-rGO aerogel was used for the construction of an electric double-layer supercapacitor. As shown in Fig. 5(a), within a potential window of 0–1 V, the CV curves of the SSC obtained at various scan rates display similar shapes, indicating an excellent volume capacitance behavior and fast charge transport. The GCD curves at different current densities also show that SSC has nearly ideal volume capacitance characteristics (Fig. 5(b)). The volume capacitance calculated according to the GCD curve is as high as 184.6 mF cm^{-3} at a current density of 2 mA cm^{-3} (Fig. 5(e)), and 61.0 mF cm^{-3} even at a very high current density of 10 mA cm^{-3}. The EIS result of the SSC shows that the R_{ct} increases obviously after 5000 cycles due to the possible polarization occurred on the electrode surface, causing the decrease in capacitance (Fig. 5(c)).[27] After 5000 charge/discharge cycles at a current density of 10 mA cm^{-3}, the SSC device can still retain a volume capacitance efficiency of 89.8% (Fig. 5(d)), which is consistent with the electrochemical impedance spectroscopy. The energy density of 32 W h kg^{-1} at power density of 1000 W kg^{-1} is advantageous when compared to those of some carbon-based composites materials,[28–33] as shown in Fig. 5(f). The insert in Fig. 5(f) is the volume energy and power densities of our SSC. It shows that the maximum volume energy density and power density are 0.5 mWh cm^{-3} and 20.0 mW cm^{-3}, respectively.

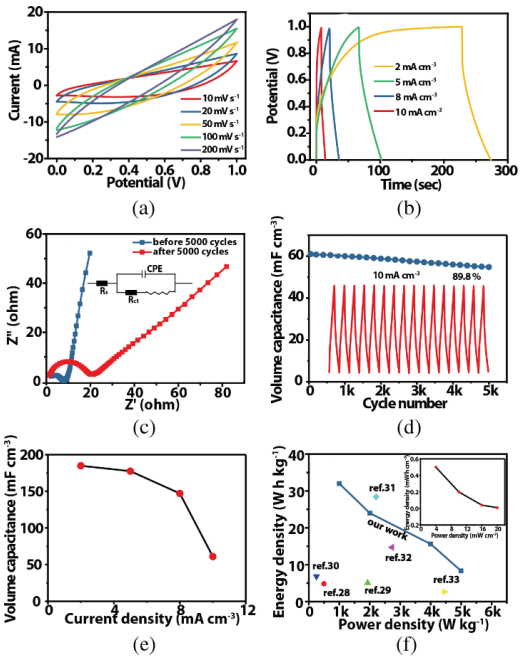

Fig. 5. Performance of all-solid-state symmetric supercapacitors: (a) CV curves at various scan rates, (b) Charge–discharge profiles at different current densities, (c) Nyquist plot of electrochemical impedance, (d) Cycling performance at 10 mAcm^{-3}, (e) Volume capacitance at different current densities, (f) Ragone plot of the SSC, the inset is volume energy and power densities.

In summary, we have successfully demonstrated a symmetrical supercapacitor based on 3D CS-rGO aerogel as the electrodes and PVA/KOH gel as the solid electrolyte. The orderly directed channels, low density, high specific surface area, high-rate electron transfer and excellent stability of CS-rGO aerogel favor its attractive electrochemical performance and also provide a potential for the use in portable carbon-based electrode materials for supercapacitor construction.

Acknowledgment

This work was supported by the Zhejiang Outstanding Youth Fund (Nos. LR19E020004 and LR20A020002).

References

1. S. Rao *et al.*, *Global Environ. Change* **42**, 346 (2017).
2. J. L. Zhang *et al.*, *Chem. Eng. J.* **396**, 125197 (2020).
3. S. Najib *et al.*, *Nanoscale* **12**, 16162 (2020).
4. M. A. Green *et al.*, *Nat. Mater.* **16**, 23 (2016).
5. S. Zhu *et al.*, *Nano Res.* **13**, 1825 (2020).
6. S. Zhu *et al.*, *Nat. Sci. Rev.* **8**, nwaa261 (2021).
7. J. Ni *et al.*, *Adv. Energy. Mater.* **6**, 1600278 (2016).
8. C. C. Hong *et al.*, *Funct. Mater. Lett.* **11**, 1850034 (2018).
9. S. Najib *et al.*, *Nanoscale Adv.* **1**, 2817 (2019).
10. A. U. Ammar *et al.*, *Beilstein J. Nanotech.* **12**, 49 (2021).
11. S. R. Tan *et al.*, *Adv. Funt. Mater.* **30**, 23 (2020).
12. S. Kasap *et al.*, *Nanoscale Adv.* **1**, 2586 (2019).
13. M. Toufani *et al.*, *Nanoscale* **12**, 12790 (2020).
14. Y. Sun *et al.*, *Nanotechnology* **32**, 19 (2021).
15. G. Hummer *et al.*, *Nature* **414**, 188 (2001).
16. S. Deville *et al.*, *Science* **311**, 515 (2006).
17. W. Z. Xu *et al.*, *ACS Nano* **13**, 7930 (2019).
18. J. Sander *et al.*, *Nat. Energy* **1**, 16099 (2016).
19. Z. Ling *et al.*, *Nanoscale* **7**, 5120 (2015).
20. N. Konstantin *et al.*, *Nano Lett.* **8**, 36 (2008).
21. G. Huang *et al.*, *Small* **21**, 3693 (2013).
22. C. Kim *et al.*, *Nano Energy* **53**, 182 (2018).

23. J. Lin *et al.*, *Nano Lett.* **13**, 72 (2012).
24. X. Xiao *et al*., *Adv. Energy Mater.* **2**, 1328 (2012).
25. W. Li *et al*., *J. Mater. Chem. A.* **5**, 16281 (2017).
26. X. Ma *et al*., *ACS Appl. Mater. Interf.* **11**, 948 (2018).
27. A. M. Engstrom *et al*., *J. Power Sources* **228**, 120 (2013).
28. B. Thomas *et al*., *J. Nanomater.* **11**, 653 (2021).
29. Y. B. Kang *et al*., *Mater. Today Commun.* **25**, 10149 (2020).
30. Y. F. Gao *et al*., *Carbon* **168**, 701 (2020).
31. X. Xiao *et al*., *Energy Environ. Sci.* **9**, 1299 (2016).
32. M. Xu *et al*., *Synthetic Metals* **267**, 116461 (2020).
33. M. Cao *et al*., *Electrochim. Acta* **345**, 1361729 (2020).

Funct. Mater. Lett. 2021.14. Downloaded from www.worldscientific.com
by ZHEJIANG UNIVERSITY OF TECHNOLOGY on 11/22/21. Re-use and distribution is strictly not permitted, except for Open Access articles.